Single-Pion Production in $\pi^- p$ Interactions at 2.26 GeV/c*

B. G. Reynolds,† J. R. Albright, R. H. Bradley, E. B. Brucker, B. C. Harms, W. C. Harrison, J. D. Kimel, J. E. Lannutti, W. H. Sims,‡ and R. P. Wieckowicz

Department of Physics, The Florida State University, Tallahassee, Florida 32306

(Received 17 December 1968)

We present an analysis of $\pi\pi N$ final states obtained from $\pi^- p$ interactions at 2.26 GeV/c. Strong ρ production is present in both final states. In addition, significant nucleon isobar production is observed. We observed the following cross sections: $\sigma(\pi^-\pi^0 p) = 3.77 \pm 0.13$ mb, $\sigma(\pi^-\pi^+ n) = 5.67 \pm 0.17$ mb, $\sigma(\rho^- p) = 2.19 \pm 0.09$ mb, $\sigma(\Delta^+(1236)\pi^-) = 0.30 \pm 0.10$ mb, $\sigma(N^0(1650)\pi^0) = 0.49 \pm 0.07$ mb, $\sigma(\rho^0 n) = 2.89 \pm 0.11$ mb, $\sigma(\Delta^-(1236)\pi^+) = 0.11 \pm 0.06$ mb, $\sigma(N^+(1470)\pi^-) = 0.24 \pm 0.06$ mb, and $\sigma(N^+(1650)\pi^-) = 0.45 \pm 0.05$ mb. The spin-density matrix elements are determined for the ρ^0 by interpreting the ρ^0 asymmetry as an interference between the resonant P wave and a $T=0$ S wave. A search for the ϵ^0 in the $\pi^+\pi^- n$ final state failed to yield a direct observation of this effect.

I. INTRODUCTION

In this article we present further work on $\pi^- p$ interactions at 2.26 GeV/c. Specifically, we were concerned with the nonstrange three-body final states $\pi^- + p \to \pi + \pi + N$. Preliminary work on the three-body final states encouraged us to double our data sample in an attempt to gain more information on resonance production.[1,2] In particular, we were interested in the detailed behavior of ρ-meson production and decay and comparison with the absorption-modified one-pion-exchange (OPEA) model,[3–6] the possible existence of a $T=0$, S-wave resonance (ϵ^0)[7] and the production of nucleon isobars in the data. Several laboratories have made studies of $\pi^- p$ interactions over a range of momenta in an attempt to study these issues.[8–26] We felt that a study using a reasonably large data sample would contribute significantly to the understanding of these problems.

This experiment consisted of $\pi^- p$ interactions obtained from an exposure of the Lawrence Radiation Laboratory 72-in. bubble chamber to a beam of 2.26-GeV/c π^- mesons. In this paper we consider the reactions

$$\pi^- p \to \pi^- p, \tag{1}$$

$$\pi^- p \to \pi^- \pi^0 p, \tag{2}$$

$$\pi^- p \to \pi^- \pi^+ n, \tag{3}$$

$$\pi^- p \to \pi^- p + \text{neutrals}, \tag{4}$$

$$\pi^- p \to \pi^- \pi^+ + \text{neutrals}. \tag{5}$$

The detailed study of elastic scattering at this energy and a discussion of the contribution of ω exchange to ρ^- production has been reported elsewhere.[27–29]

* Research supported in part by the U. S. Atomic Energy Commission.

† Present address: Department of Physics, Ohio University, Athens, Ohio 45701.

‡ Present address: Physics Department, Brookhaven National Laboratory, Upton, N. Y. 11973.

[1] B. G. Reynolds, Florida State University High-Energy Physics Report No. FSU-HEP-66-8-1, 1966 (unpublished).

[2] B. G. Reynolds, J. R. Albright, B. C. Harms, W. C. Harrison, and J. E. Lannutti, Bull. Am. Phys. Soc. **11**, 841 (1966).

[3] K. Gottfried and J. D. Jackson, Nuovo Cimento **34**, 735 (1964); J. D. Jackson, Rev. Mod. Phys. **37**, 484 (1965); J. D. Jackson, J. T. Donohue, K. Gottfried, R. Keyser, and B. E. Y. Svensson, Phys. Rev. **139**, B428 (1965).

[4] M. H. Ross and G. L. Shaw, Phys. Rev. Letters **12**, 627 (1964).

[5] L. Durand and Y. T. Chiu, Phys. Rev. **137**, B1530 (1965).

[6] J. G. Wills, D. Ellis, and D. B. Lichtenberg, Phys. Rev. **143**, 1375 (1960).

[7] L. Durand and Y. T. Chiu, Phys. Rev. Letters **14**, 329 (1965).

[8] Saclay-Orsay-Bari-Bologna Collaboration, Nuovo Cimento **29**, 515 (1963).

[9] Saclay-Orsay-Bari-Bologna Collaboration, Nuovo Cimento **25**, 365 (1962).

[10] Saclay-Orsay-Bari-Bologna Collaboration, Nuovo Cimento **35**, 713 (1965).

[11] V. Hagopian and W. Selove, Phys. Rev. Letters **10**, 533 (1963).

[12] V. Hagopian, W. Selove, J. Alitti, J. P. Baton, and N. Neveu-Rene, Phys. Rev. **145**, 1128 (1966).

[13] Zaven G. T. Guiragossian, Phys. Rev. Letters **11**, 85 (1963).

[14] Aachen-Birmingham-Bonn-Hamburg-London (I. C.)-München Collaboration, Nuovo Cimento **31**, 729 (1964).

[15] D. H. Miller, L. Gutay, P. B. Johnson, F. J. Loeffler, R. L. McIlwain, R. J. Sprafka, and R. B. Willmann, Phys. Rev. **153**, 1423 (1967).

[16] R. L. Eisner, P. B. Johnson, P. R. Klein, R. E. Peters, R. J. Sahni, W. L. Yen, and G. W. Tautfest, Phys. Rev. **164**, 1699 (1967).

[17] E. West, J. H. Boyd, A. R. Erwin, and W. D. Walker, Phys. Rev. **149**, 1089 (1966).

[18] Vasken Hagopian and Yu-Li Pan, Phys. Rev. **152**, 1183 (1966).

[19] I. Derado, J. A. Poirier, N. N. Biswas, N. M. Cason, V. P. Kenney, and W. D. Shephard, Phys. Letters **24B**, 112 (1967).

[20] D. R. Clear, T. F. Johnson, J. Plicher, J. D. Prentice, N. R. Steenberg, E. West, T. S. Yoon, W. A. Cooper, W. Manner, L. Voyvodic, and W. D. Walker, Nuovo Cimento **49**, 399 (1967).

[21] D. D. Allen, G. P. Fisher, G. Godden, J. B. Kopelman, L. Marshall, and R. Sears, Phys. Rev. Letters **17**, 53 (1966).

[22] D. Huwe, E. Marquit, F. Oppenheimer, W. Schultz, and J. R. Wilson, Phys. Letters **24B**, 252 (1967).

[23] W. E. Schultz, thesis, University of Colorado, 1968 (unpublished).

[24] L. D. Jacobs, University of California Radiation Laboratory Report No. UCRL-16877, 1966 (unpublished).

[25] J. P. Baton, G. Laurens, and J. Reignier, Phys. Letters **25B**, 419 (1967); Nucl. Phys. **B3**, 349 (1967).

[26] J. P. Baton and G. Laurens, Phys. Letters **26B**, 471 (1968).

[27] B. G. Reynolds, J. R. Albright, E. B. Brucker, W. C. Harrison, B. C. Harms, J. D. Kimel, and J. E. Lannutti, Phys. Letters **24B**, 311 (1967).

[28] B. G. Reynolds, J. D. Kimel, J. R. Albright, R. H. Bradley, E. B. Brucker, B. C. Harms, W. C. Harrison, J. E. Lannutti, W. H. Sims, and R. P. Wieckowicz, Phys. Rev. **173**, 1403 (1968).

[29] B. G. Reynolds, J. R. Albright, R. H. Bradley, E. B. Brucker, B. C. Harms, W. C. Harrison, J. E. Lannutti, W. H. Sims, and R. P. Wieckowicz, Nucl. Phys. **B6**, 633 (1968).

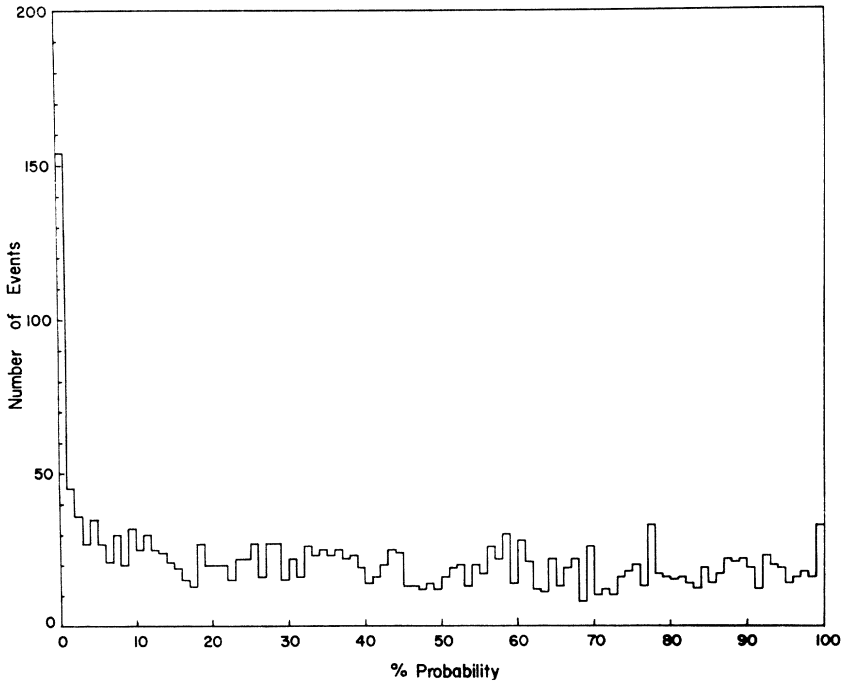

FIG. 1. χ^2 probability distribution for events fitting the $\pi^-\pi^0 p$ final state.

II. EXPERIMENTAL DETAILS

We have scanned approximately 10 000 pictures and found a total of 15 482 events with two charged secondaries. These events were measured on film-plane measuring machines, and geometric reconstruction and kinematic fitting were accomplished using the University of California Lawrence Radiation Laboratory PANAL and PACKAGE programs. PACKAGE attempted to fit each of the five hypotheses represented by reactions (1)–(5). In addition, strange-particle hypotheses were tried by PACKAGE in an attempt to filter out obvious associated production events. Output from PACKAGE for each event was tested for measurement quality, and any difficulties in reconstruction and fitting were noted. Events that were considered to be poorly measured or failed to reconstruct properly were remeasured. There were 956 events that failed to pass the quality and reconstruction tests after three measurements. A careful study revealed that the exclusion of these events from the data introduced no biases and they were deleted.[28] A fiducial volume restriction removed 740 events from our sample, leaving a total of 13 786 two-prong events for further analysis.

The events accepted were assigned to one or more of the reactions (1)–(5) on the basis of χ^2. A discussion of the assignment of events to reaction (1) has been given elsewhere.[28] In addition, 438 events were classified as associated production events on the basis of topology, PACKAGE output information, and ionization. The remaining events were considered to fit either hypothesis (2) or (3) (or both) if they had a χ^2 probability $\geq 0.1\%$. Events that failed to meet this requirement were classified as multiple neutral reactions, i.e., hypothesis (4) or (5). Events that were ambiguous between hypotheses (2) and (3) and all of the multiple neutral events were assigned to the correct hypothesis using the ionization of the positive track. This ionization technique was useful only when the momentum of the positive track was less than 1200 MeV/c. For positive tracks with a higher momentum, it was impossible to distinguish a π^+ from a proton. There were 267 events that were ambiguous between hypotheses (2) and (3). A study of these events indicated that at least 80% of these events should be assigned to hypothesis (3). The various effective-mass spectra and c.m. angular distributions strongly favored this interpretation. As a result of this analysis, we assigned all of the 267 ambiguous events to hypothesis (3). A similar study of 290 events, with positive track momentum greater than 1200 MeV/c, which were ambiguous between hypotheses (4) and (5), resulted in the assignment of all 290 events to hypothesis (5).

After the events were assigned to hypotheses (1)–(5), as indicated above, there remained the problem of removing multiple neutral events from reactions (2) and (3). This problem occurs when an interaction of type (4) erroneously fits hypothesis (2). Similarly, type-(5) reactions tend to contaminate the type-(3) events. A reasonably accurate estimate of the amount of contamination was obtained using the χ^2 probability and unfitted missing-mass distributions for reactions (2) and (3). The χ^2 probability distributions for reactions (2) and (3) are given by Figs. 1 and 2, respectively. The distributions of the square of the unfitted missing

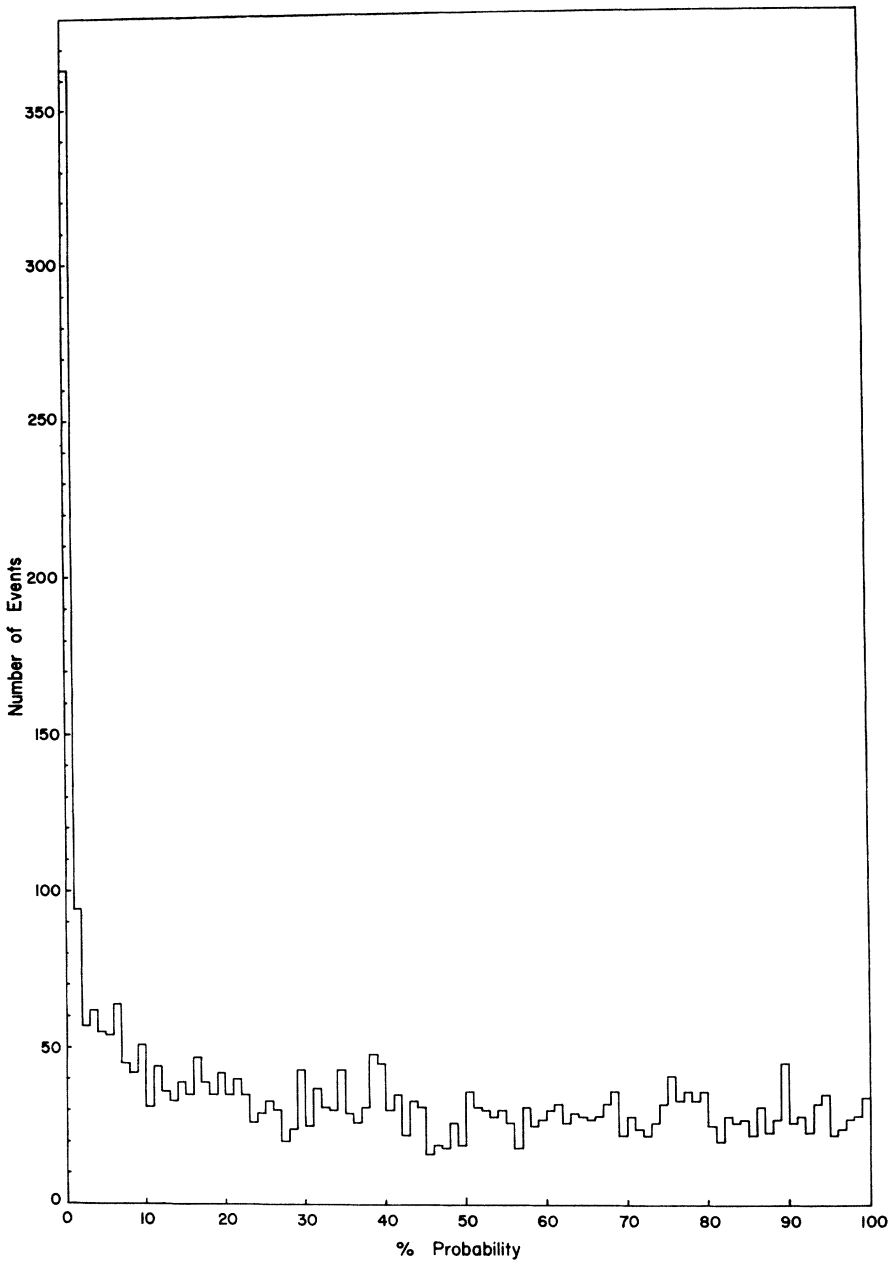

FIG. 2. χ^2 probability distribution for events fitting the $\pi^-\pi^+n$ final state.

mass are given in Figs. 3 and 4. The shaded regions in Figs. 3 and 4 correspond to events already assigned to the multiple neutral catagories. Two points are of interest: (a) the large number of events with probability less than 2%, and (b) the asymmetric distribution of the square of the unfitted missing mass about the mass of the π^0 in Fig. 3 and about the neutron mass in Fig. 4. Both of these effects are attributed to the existence of multiple neutral events in the data sample.

A study of these two types of distributions revealed that the events with probability $\leq 10\%$ were responsible for the asymmetry in the mass-squared plots. Two methods were used to estimate the number of type-(4) events in the type-(2) sample and the number of type-(5) events in the type-(3) sample. First, because we believed that the proper error settings had been made in PACKAGE, we required that the probability distribution be flat. This method provided an estimate of the number of multiple neutral events in the one-constraint data. Second, we required that the missing-mass-squared distributions be symmetric about the value of the expected missing mass squared. This procedure involved taking into account the asymmetric nature of the beam momentum distribution, which

TABLE I. Final-state cross sections for π^-p interactions at 2.26 GeV/c.

Final state	No. of events (corrected)	Cross section (mb)
π^-p	5 268	8.91±0.24
$\pi^-\pi^0p$	2 232	3.77±0.13
$\pi^-\pi^+n$	3 344	5.67±0.17
π^-p^+ neutrals	1 019	1.71±0.07
$\pi^-\pi^+$+neutrals	3 936	6.66±0.19
Strange particles (two-prong)	438	0.75±0.04
Total two-prong	16 237	26.75±0.56
Total zero-prong	2 446	3.94±0.13
Total four-prong	2 501	4.04±0.13
Total	21 184	35.48±0.25

tends to introduce a slight asymmetry into the mass-squared distributions.

The two methods gave estimates of multiple neutral contamination that were in agreement. We concluded that the events with χ^2 probability $\leq 10\%$ were contaminated by multiple neutral events, while the events with χ^2 probability greater than 10% were essentially free of this contaminant. For the purpose of cross-section determinations, the event counts for hypotheses (4) and (5) were corrected by the above methods. 237 events were transferred from reaction (2) to reaction (4), and 648 events were transferred from (3) to (5).

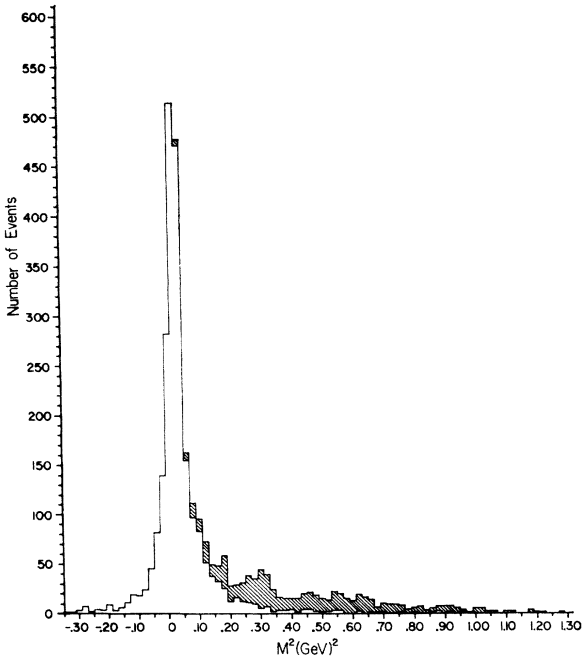

FIG. 3. Square of the unfitted missing mass for events fitting the $\pi^-\pi^0p$ final state. The shaded events are those accepted as fitting the π^-p +neutrals final state.

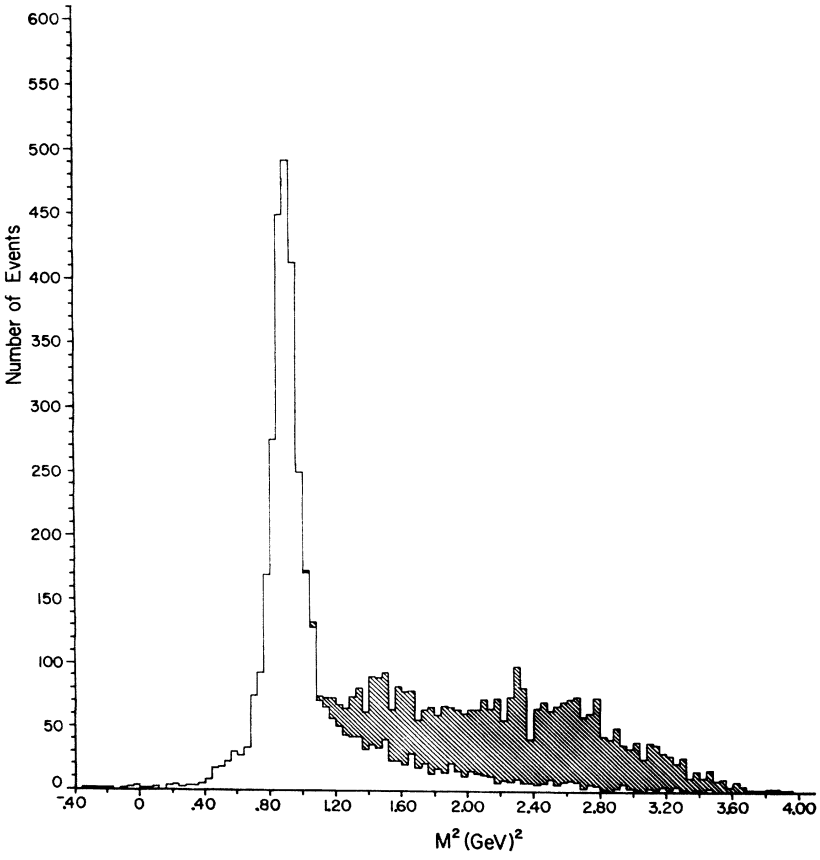

FIG. 4. Square of the unfitted missing mass for events fitting the $\pi^-\pi^+n$ final state. The shaded events are those accepted as fitting the $\pi^-\pi^+$ +neutrals final state.

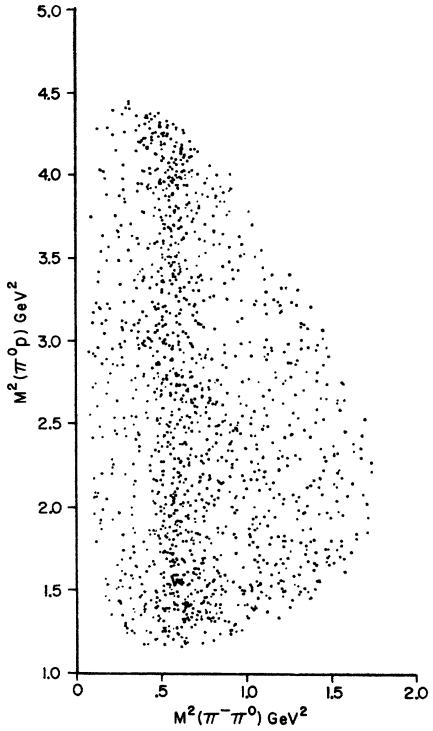

FIG. 5. Dalitz plot for the $\pi^-\pi^0 p$ final state.

III. FINAL-STATE CROSS SECTIONS

In order to determine the cross sections for reactions (1)–(5), we have double-scanned the film for events with zero-, two-, and four-prong topologies. This scanning procedure enabled us to determine a scan efficiency for each event topology. The total event count, after corrections for scanning bias against short recoil protons and scanning efficiency, was normalized to the total $\pi^- p$ cross section interpolated from Diddens *et al.*[30] A detailed account of the elastic scattering bias corrections has been given elsewhere.[28] A similar procedure was used to correct the number of type-(2) events. The cross sections for each two-prong final state and for the other topologies are given in Table I. The errors in the quoted values of these cross sections reflect only the statistical uncertainties in our data sample and in the total cross-section value used.

IV. RESONANCE PRODUCTION

A. General Features of $\pi^-\pi^0 p$ and $\pi^-\pi^+ n$ Final States

In order to remove the effects of contamination due to multiple neutral events, the following selections were made: for the $\pi^-\pi^0 p$ final state, $P(\chi^2)\geq 10\%$ and $-0.06\leq$ (missing mass)$^2\leq 0.11$ GeV^2; and for the $\pi^-\pi^+ n$ final state, $P(\chi^2)\geq 10\%$ and $0.68\leq$ (missing mass)$^2\leq 1.10$ GeV^2. These selections further reduced the data sample to 1517 type-(2) events and 2242 type-(3) events.

Two Dalitz plots for reaction (2) are given in Figs. 5 and 6. In both plots ρ^- production is seen to be the dominant effect. Two additional concentrations of points are also apparent. In Fig. 5 there is a cluster of points corresponding to low $\pi^0 p$ mass. Figure 6 shows a band corresponding to the 1650-MeV $\pi^- p$ mass region. These effects are even more striking when the data are displayed in the three effective-mass spectra given by Figs. 7–9. The Dalitz plots and effective-mass plots for reaction (3) are given in Figs. 10–14. Here, the ρ^0 is seen to be the dominant feature of this final state. The decay asymmetry of the ρ^0 is also apparent in both Dalitz plots. The $\pi^-\pi^+ n$ final state is also seen to have structure in the π-nucleon mass spectra. The $\pi^+ n$ effective-mass distribution in Fig. 14 indicates three possible isobars in the 1240-, 1470-, and 1650-MeV mass regions. The peripheral nature of ρ production in both charge states is illustrated by the Chew-Low plots in Figs. 15 and 16.

Isobar production has been studied in several experiments in the incident momentum interval 1.5–4.0 GeV/c.[10,15–17,20] The conclusions drawn from these experiments indicate the need for further study of isobar production in this energy region. In general, there does seem to be some $\Delta(1236)$ production. Moreover, there have been varying reports of $\Delta(1920)$ production.[17] A detailed study of the reality of these effects is hampered by the distortion effects from ρ

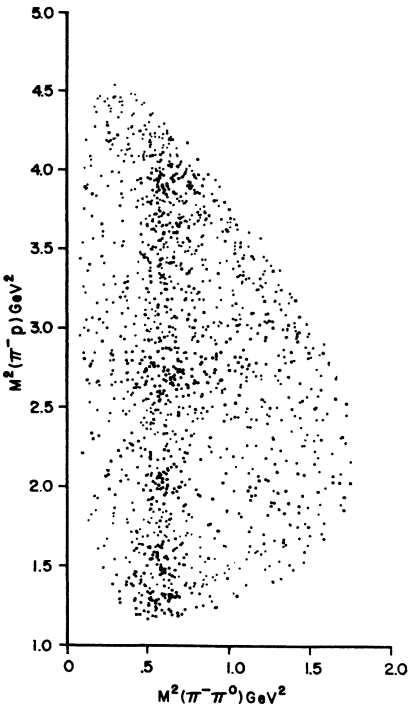

FIG. 6. Dalitz plot for the $\pi^-\pi^0 p$ final state.

[30] A. N. Diddens, E. W. Jenkins, T. F. Kycia, and K. F. Riley, Phys. Rev. Letters **10**, 262 (1963).

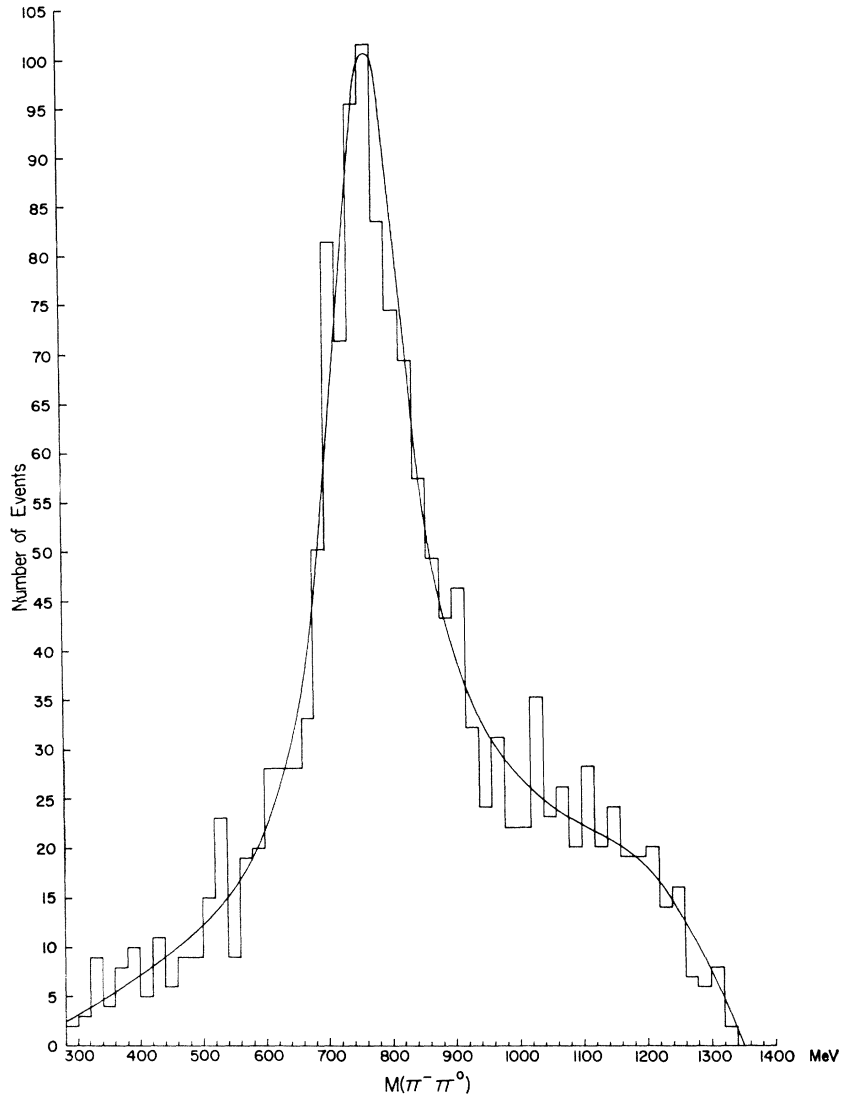

FIG. 7. Effective mass of the $\pi^-\pi^0$ system from the $\pi^-\pi^0 p$ final state.

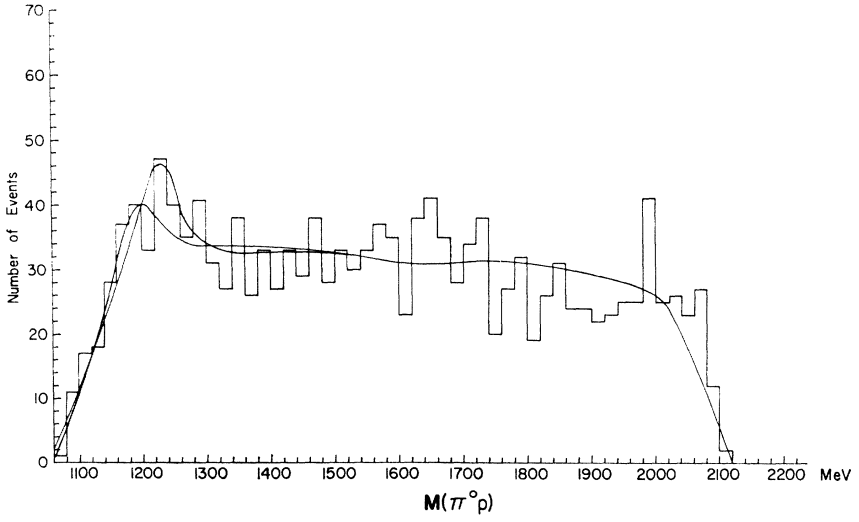

FIG. 8. Effective mass of the $\pi^0 p$ system from the $\pi^-\pi^0 p$ final state.

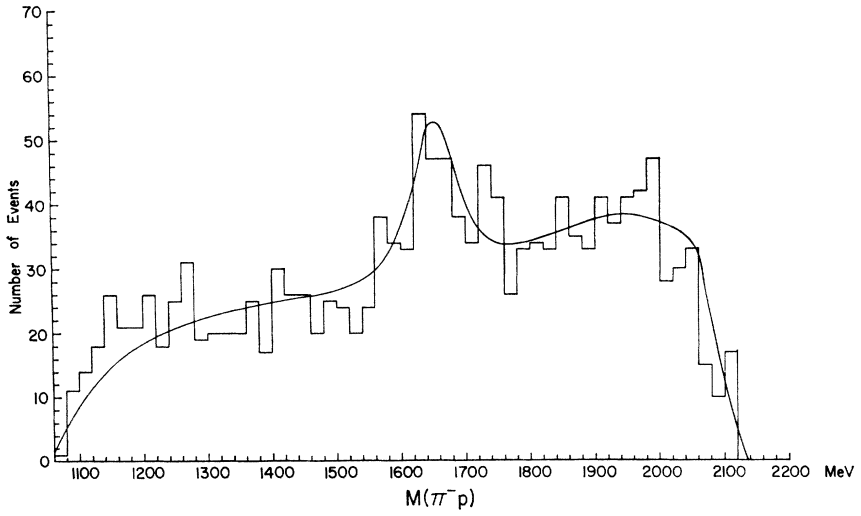

FIG. 9. Effective mass of the π^-p system from the $\pi^-\pi^0p$ final state.

production. More recently, resonance production effects have been reported in π-nucleon mass spectra in the region of 1650 MeV.[15,16] This effect can be attributed to any one of three reported resonances.[31]

In order to study isobar production in our data and obtain estimates of the resonance cross sections, we have fitted the effective-mass distributions to a model consisting of Breit-Wigner resonance shapes and incoherent phase-space background. The form used for the Breit-Wigner distributions was that suggested in Ref. 32:

$$\phi_R(\omega)=\frac{\omega}{q}\frac{\Gamma(\omega)}{(\omega_0^2-\omega^2)^2+\omega_0^2\Gamma^2(\omega)}, \tag{6}$$

where the energy-dependent width $\Gamma(\omega)$ is given by

$$\Gamma(\omega)=\Gamma_0(q/q_0)^{2l+1}f(\omega)/f(\omega_0). \tag{7}$$

In expressions (6) and (7), ω is the diparticle invariant mass, q is the three-momentum of either particle in the diparticle rest frame, and Γ_0, ω_0, and q_0 are the values of the width, mass, and three-momentum at the resonance mass; $f(\omega)$ is a function that depends on the

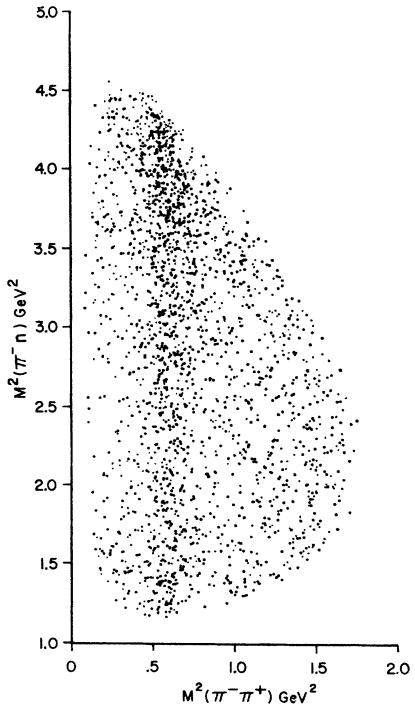

FIG. 10. Dalitz plot for the $\pi^-\pi^+n$ system.

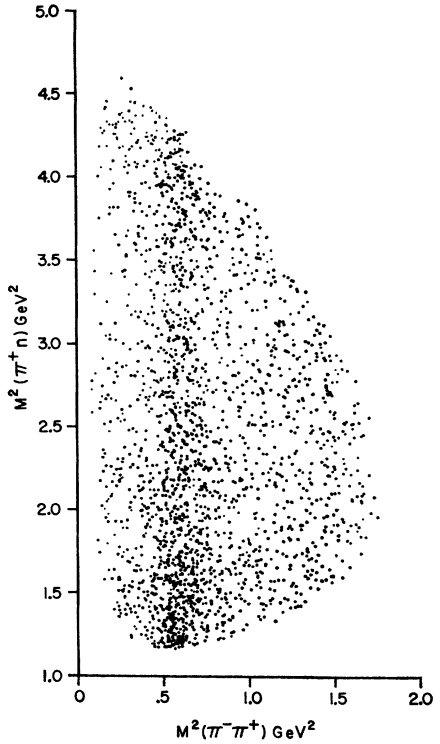

FIG. 11. Dalitz plot for the $\pi^-\pi^+n$ system.

[31] A. H. Rosenfeld, N. Barash-Schmidt, A. Barbaro-Galtieri, L. R. Price, Paul Söding, C. G. Wohl, M. Roos, and W. J. Willis, Rev. Mod. Phys. **40**, 77 (1968).

[32] J. D. Jackson, Nuovo Cimento 34, 1644 (1964).

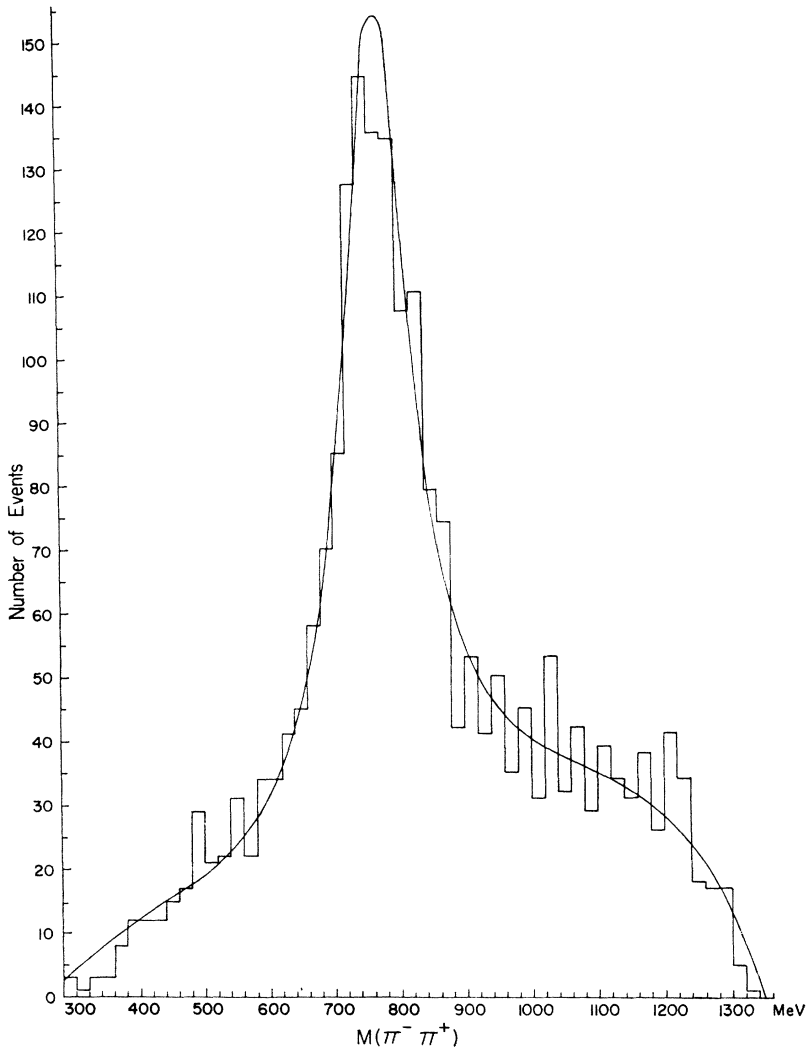

FIG. 12. Effective mass of the $\pi^-\pi^+$ system from the $\pi^-\pi^+n$ final state.

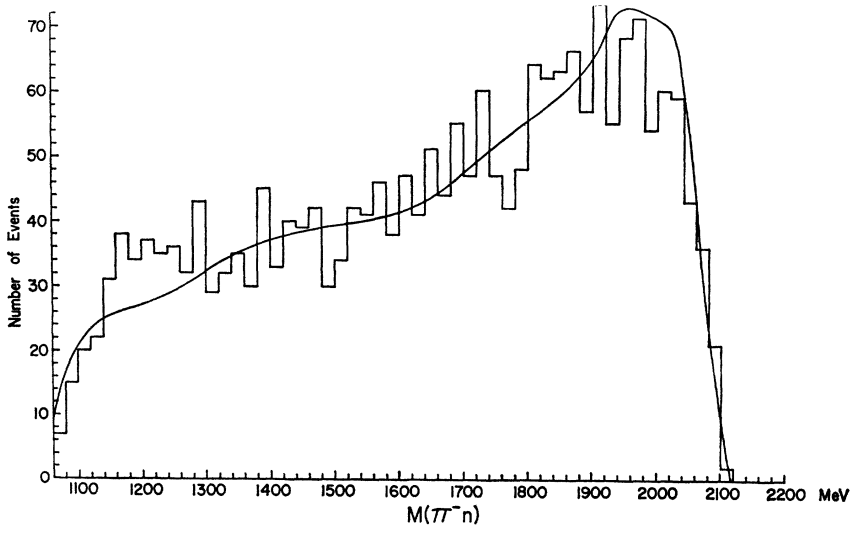

FIG. 13. Effective mass of the π^-n system from the $\pi^-\pi^+n$ final state.

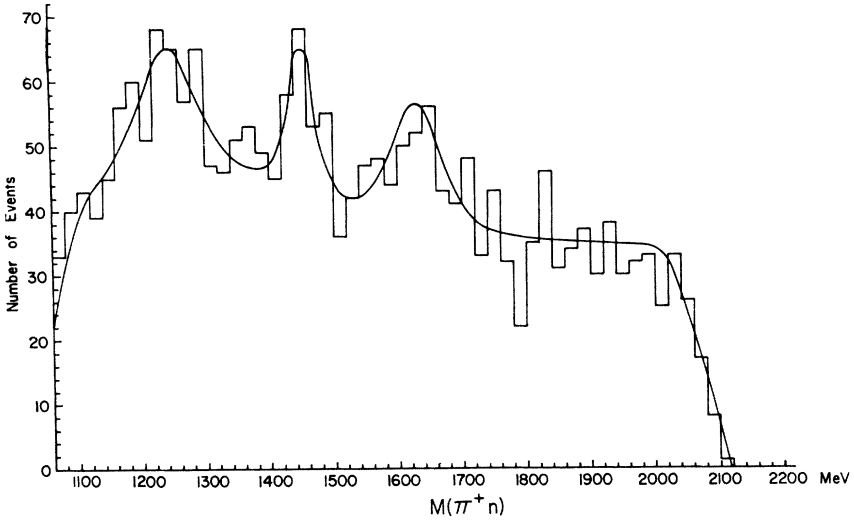

FIG. 14. Effective mass of the π^+n system from the $\pi^-\pi^+n$ final state.

particular resonance in question. For the ρ, the form of $f(\omega)$ used was $1/\omega$.[32] The symbol l represents the relative orbital angular momentum of the two particles in the diparticle rest frame. A complete discussion of the formulation used here has been given by Jackson.[32]

For the purpose of fitting the mass spectra, we began with the dipion mass distributions (Figs. 7 and 12). We fitted them to a model which contained phase space plus the Breit-Wigner form of Eq. (6); the variables were ω_0 and Γ_0 for the ρ^0 and the ρ^-, as well as the relative amounts of resonance and phase space. The resulting values of the position and width of each ρ, along with the angular distributions for production and decay (as observed in this experiment), were used in a Monte Carlo program to generate pion-nucleon mass spectra to be applied to Figs. 8, 9, 13, and 14. The next step was to fit these four mass spectra to a model involving phase space, ρ background from the Monte Carlo program, $\Delta(1236)$, and (where applicable) resonant forms near 1470 and 1650 MeV; the variables in the fit were the relative amounts of each part of the model and the values of Γ_0 and ω_0 for each pion-nucleon resonance. Equation (6) was used for the $\Delta(1236)$; a simple Breit-Wigner with constant width was used for the 1470 and 1650 peaks. The resulting positions and widths from this fit were in turn used as input to the Monte Carlo program, which produced the appropriate reflection curves for the opposite pion-nucleon spectrum

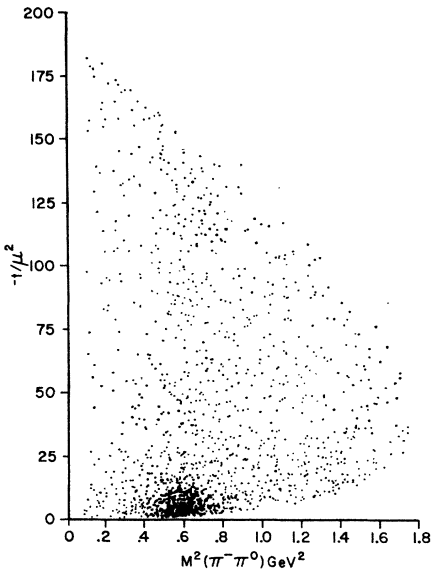

FIG. 15. Chew-Low plot of the squared four-momentum transfer to the proton $(-t/\mu^2)$ versus $M^2(\pi^-\pi^0)$ from the $\pi^-\pi^0p$ final state.

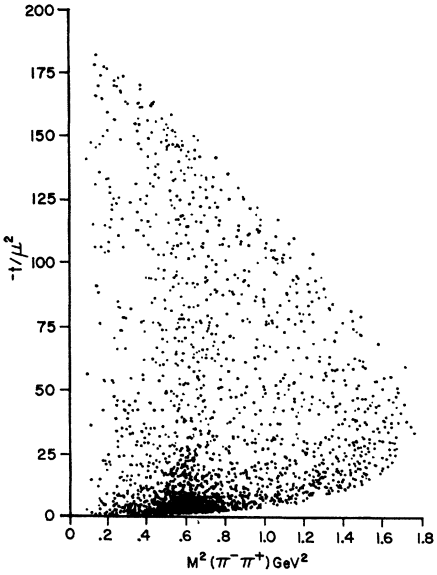

FIG. 16. Chew-Low plot of the squared four-momentum transfer to the neutron $(-t/\mu^2)$ versus $M^2(\pi^-\pi^+)$ from the $\pi^-\pi^+n$ final state.

and for the dipion spectrum. The last step was to do a fit to all six mass spectra simultaneously. The masses and widths previously determined were held fixed, and the relative amounts of each part of the model were permitted to vary. The results are shown as the smooth curves in Figs. 7–9 and 12–14. Typically the χ^2 for each mass plot taken separately was of the order of 50 with 50 degrees of freedom. Several interesting features of resonance production in these spectra, as well as our method of estimating cross sections, are given fuller discussion in the following paragraphs.

B. Resonance Production in $\pi^-\pi^0p$ Final State

The results of the combined fit to the three effective-mass distributions in Figs. 7–9 are displayed as solid lines on these figures. The numerical results are presented in Table II. The model used in the fitting assumed that the data can be reproduced by an incoherent superposition of ρ^-, $\Delta(1236)$, $N(\simeq 1650)$, and phase space. The best-fit solutions are the ones given in Table II. When energy-independent and energy-dependent [with various forms of $f(\omega)$] Breit-Wigner shapes were used in the fitting, the parameters Γ_0 and ω_0 were found to change appreciably. However, the percentages of the contributing resonances were essentially the same for all fits. Thus, while this technique is most useful for determining resonance cross sections, care must be taken in assigning physical significance to the corresponding values of Γ_0 and ω_0. The best-fit model curves are in reasonable agreement with the data. $\Delta^+(1236)$ production is seen in Fig. 8. Here we have displayed the results of an energy-dependent (lower curve) and an energy-independent (upper curve) Breit-Wigner fit. The principal disagreements between the data and the model occur in the region of 1550–1750 MeV and the shoulder around 2100 MeV.

Figure 9 indicates that isobar production is present in the π^-p mass region of 1650 MeV. We have labeled this effect $N^0(1650)$ since all fits gave a value of ω_0 near 1650 MeV. It should be noted that a slightly better χ^2 is obtained if we allow for the presence of $\Delta^0(1236)$ and $N^0(1470)$ production in the π^-p effective-mass distribution. The presence of these resonances is suggested by the data but the statistical significance of these effects is negligible. Thus, for the purposes of this data presentation we have neglected these effects in the determination of resonance production cross sections. The inclusion of these resonances in Table II and their mention here is for purposes of comparison with similar enhancements in the $\pi^-\pi^+n$ final state. The excess of events above the model curves in the region of 1950 MeV is not considered to be of statistical significance. One is always suspicious of mass enhancements that take place at the extremes of π-nucleon mass distributions in conjunction with ρ production. In this analysis, the Monte Carlo event simulation, by necessity, contained a fraction of nonresonant (non-ρ^-) background. Any inability to parametrize the ρ^- angular distributions correctly will show up in the reflected π-nucleon mass distributions. In this experiment the $\Delta(1236)$ and $\Delta(1920)$ mass regions are most sensitive to this problem, and any overestimation or underestimation of the "true" ρ decay distributions will severely affect these mass regions. This was particularly a problem with the two decay modes of the $\Delta^+(1236)$ accessible in this experiment. Here we invoked charge independence as a constraint in our cross-section determinations and required

$$R(\Delta^+ \to \pi^0p)/(R\Delta^+ \to \pi^+n) = 2/1\,.$$

Table III shows the expected branching ratios obtained from a $T=1$ exchange model of isobar production. We see that, within the statistical accuracy of this experiment, the $\Delta(1236)$ in the $\pi^-\pi^0p$ final state is consistent with this model. Furthermore, the strong effect in the 1650-MeV region of the π^-p effective-mass plot, together with the lack of significant structure in the 1600–1700-MeV mass region of the π^0p effective-mass plot, indicates that this effect is due to an $N(1650)$ rather than a $\Delta(1650)$. Two such N resonances have been reported in the 1670-MeV mass region.[31] It is worthwhile to mention that any $N(1470)$ production via a $T=1$ exchange mechanism should appear most pronounced in the π^-p effective-mass distribution and should be less obvious in the π^0p plot. We see no evidence of an enhancement in the 1470-MeV region in Fig. 8 and only a slight indication of a 1470-MeV effect in Fig. 9.

TABLE II. Resonance cross sections in $\pi\pi N$ final states from π^-p interactions at 2.26 GeV/c.

Final state	Resonance	Fraction (%)	Cross section (mb)
$\pi^-\pi^0p$	ρ^-	58.1±2.5	2.19±0.09
	$\Delta^+(1236)$	5.4±1.1	0.20±0.06
	$\Delta^0(1236)$	not estimated	
	$N^{*0}(1470)$	not estimated	
	$N^{*0}(1650)$	12.9±1.8	0.49±0.07
$\pi^-\pi^+n$	ρ^0	50.9±2.0	2.89±0.11
	$\Delta^+(1236)$	1.7±0.9	0.10±0.07
	$\Delta^-(1236)$	2.0±1.0	0.11±0.06
	$N^{*+}(1470)$	4.3±1.0	0.24±0.06
	$N^{*+}(1650)$	8.0±1.0	0.45±0.05

TABLE III. Relative cross sections for nucleon isobars produced by a $T=1$ exchange model.

Resonance	$\sigma(\pi^0p)$	$\sigma(\pi^-p)$	$\sigma(\pi^-n)$	$\sigma(\pi^+n)$
$\Delta(1236)$	4	1	0	2
$N^*(1470)$	1	4	0	2
$N^*(1650)$	1	4	0	2
$\Delta(1650)$	4	1	0	2

TABLE IV. ρ mass and width parameters obtained by fitting mass spectra.

Resonance	Combined mass fit ω_0 (MeV)	Combined mass fit Γ_0 (MeV)	$\pi\pi$ mass fit ω_0 (MeV)	$\pi\pi$ mass fit Γ_0 (MeV)
ρ^-	776±4	151±10	778±4	157±10
ρ^0	771±3	127±7	774±3	143±8

C. Resonance Production in $\pi^-\pi^+n$ Final State

Resonance production in the $\pi^-\pi^+n$ final state and the corresponding best-fit model curves are exhibited in Figs. 12–14. Production of the f^0 meson is kinematically inhibited at this energy, and there is no significant evidence of f^0 in the 1250-MeV mass region of Fig. 12. In addition to ρ^0 production in Fig. 12, the π^-n effective-mass plot shows an enhancement above the model curve in the region of 1230 MeV. As indicated in Table III, this effect in the $\Delta^-(1236)$ mass region cannot be ascribed to a simple $T=1$ exchange mechanism by charge conservation. Similar effects have been reported in other experiments.[20] One is again reminded of the distortion effects due to ρ^0 production and the sensitivity of the model in the extreme π-nucleon mass regions to an accurate parametrization of the ρ angular distributions. However, since the fit of our model to the rest of the $\pi^-\pi^+n$ final state seems reasonable, we are inclined to accept this π^-n enhancement at 1236 MeV as real and not an underestimate in the model parametrization. A $\pi\Delta(1236)$ decay mode of the nearby s-channel $N(2190)$ would contribute most heavily to $\Delta(1236)\rightarrow\pi^-n$ and thus, because of the close proximity of this well-established resonance, a postulated cascade mechanism could provide a possible explanation of the π^-n mass enhancement at 1236 MeV.[31] The cross section is given in Table II.

The π^+n mass spectrum suggests three examples of isobar production, all of which are allowed by a $T=1$ exchange model. Assuming such a model, a comparison with resonance production in the $\pi^-\pi^0p$ final state can be made. Table III indicates that $\Delta(1236)$ production would occur in the π^0p and π^+n plots, and in the π^-p mass plot to a lesser extent. This is in agreement with our cross-section determination. The $N(1650)$ is also in qualitative agreement with Table III but fails to meet the $\pi^-p:\pi^+n:\pi^0p=4:2:1$ requirement of a $T=1$ exchange model. The qualitative comparison of the different charge states of $N(1470)$ is less impressive. Indications of this effect are totally absent in the π^0p mass distribution of Fig. 8. The most pronounced effect should appear in the π^-p mass plot. However, we see only a slight suggestion of $N(1470)$ production. The strongest support for the $N(1470)$ is obtained in the π^+n mass distribution. Similar behavior is noted by Eisner *et al.* in an experiment at 4.16 GeV/c, where a 1470-MeV mass enhancement is most visibly pronounced in the π^+n mass spectrum.[16] The large background in all isobar mass regions prohibits detailed analysis of isobar angular distributions.

We further note, for the purpose of comparison, the ρ-production ratio predicted by the OPEA model[3] is $\sigma(\rho^0):\sigma(\rho^-)=2:1$. Our experimental value is $\simeq 1.3:1.0$, as shown in Table II, and is in disagreement with the OPEA-model prediction. There are three experimental facts that must be considered in any attempt to discuss this discrepancy with the OPEA model. First, the c.m. energy of this experiment is only 70 MeV away from the $N(2190)$,[31] and s-channel effects on the three-body final states due to this 8-mb effect cannot be ruled out *a priori*. Second, it has already been shown that the ρ^- production and decay angular distribution cannot always be completely described by the OPEA model.[16,29] This fact allows speculation as to the possible effects of the other allowed exchange particles. A previous analysis has shown that the assumption of ω exchange is not simultaneously compatible with both the production and decay angular distribution of the ρ^- in this experiment.[29] Third, there are currently three experiments with rather good statistics at 2.10, 2.26, and 2.36 GeV/c. The experiment at 2.10 GeV/c has been reported by West *et al.*[17] The experiment at 2.36 GeV/c was conducted by Schultz.[23] The corresponding c.m. energies of these three experiments are 2.20, 2.27, and 2.31 GeV, respectively. As such, the total spread in c.m. energy is less than one pion mass. The close proximity of these experiments to the reported position of the $N(2190)$ should show what effect, if any, the formation and subsequent decay of this resonance have on the $\pi\pi N$ final states. Furthermore, one would expect that any deviations from an OPEA mechanism for ρ production should manifest itself in approximately the same fashion in all three experiments.

The experiments at 2.26 and 2.36 GeV/c show a substantial deviation from the 2:1 ratio of the OPEA model. This effect has also been seen by Miller *et al.* at 2.7 GeV/c.[15] However, the experiment at 2.1 GeV/c is in good agreement with the 2:1 ratio. Further comparison of the results of these three experiments indicates that it is not possible to obtain consistent agreement on several key issues such as partial cross sections, fraction of resonance production in a given final state, and relative amount of multiple neutral production. Thus the attempt to study the effects of the $N(2190)$ and deviation from the OPEA mechanism in the $\pi\pi N$ final states at this energy are frustrated, to a degree, by the disagreement among these three experiments.

We have attempted to analyze this problem in terms of models for $N(2190)\rightarrow\rho N$ as well as ω exchange as a contributor to ρ production. We find nothing in any of these results that would enable us to make compelling arguments for either model.

V. ϱ-MESON PRODUCTION AND DECAY

A. ϱ-Meson Production

The correlation between dipion mass squared and the squared four-momentum transfer to the nucleon $-t$ is given by the Chew-Low plots in Figs. 15 and 16. These plots indicate that both charge states of the ρ are produced in the 0.6-GeV^2 region by a highly peripheral mechanism. Although both plots show that the majority of the ρ mesons are produced with $-t \leq 20\mu^2$, the effect of the ρ continues into the region of larger values of $-t$. The quantity μ is the pion mass.

In order to study the details of ρ production and decay, a more restrictive selection of events was necessary. The results of the mass-fitting procedure (Sec. IV) for both charge states of the ρ are given in Table IV. These are the results obtained both by simultaneously fitting all three mass spectra for each final state (combined mass fit) and by fitting only the $\pi\pi$ mass spectrum ($\pi\pi$ mass fit) from each final state. The values of ω_0 obtained by the two methods are in agreement. There is some variation in the values for Γ_0. This pattern was also observed when the ρ mass and width parameters were determined for various regions of $-t$. Again the values of ω_0 were in agreement for each charge state of the ρ. However, the width parameter Γ_0 changed appreciably as a function of $-t$, with the ρ^0 fits being most subject to fluctuation. In our analysis we have selected events with $680 \leq M(\pi\pi) \leq 880$ MeV as being representative of both charge states of the ρ. This selection yielded 738 $\pi^-\pi^0$ events and 991 $\pi^-\pi^+$ events. In what follows, we shall always mean events from this mass region unless otherwise specified.

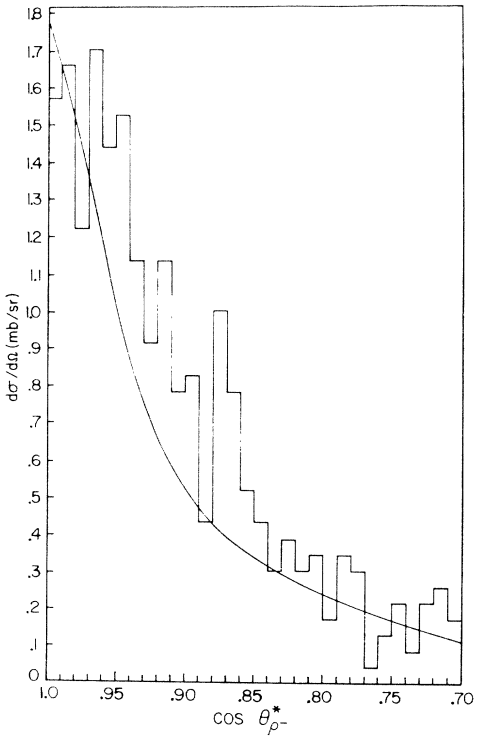

FIG. 17. ρ^- differential production cross section as a function of $\cos\theta_{\rho^-}{}^*$. The solid curve is the OPEA-model prediction.

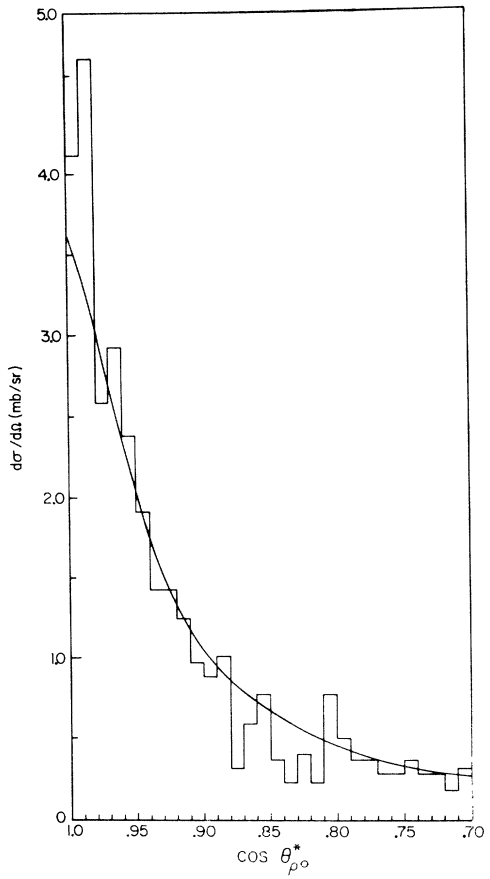

FIG. 18. ρ^0 differential production cross section as a function of $\cos\theta_{\rho^0}{}^*$. The solid curve is the OPEA-model prediction.

The OPEA model has been very successful in predicting the production and decay angular distributions for $\rho^{0,-}$ mesons produced in quasi-two-body final states.[3-6] A comparison of this model with the differential production cross sections as a function of $\cos\theta_\rho{}^*$, the cosine of the ρ c.m. production angle, is given in Figs. 17 and 18. The solid curve is the OPEA-model prediction in each figure. These curves were calculated at this energy using a fit to our elastic scattering data.[27,28] The initial-state absorption parameters resulting from this fit were $C_+=0.827$ and $\gamma_+=0.065$. The final-state absorption parameters were chosen to be $C_-=1.0$ and $\gamma_-=\frac{3}{4}\gamma_+$.[3] It should be noted that our value of $\sigma(\rho^0)/\sigma(\rho^-)=1.3$ necessitated normalization of the experimental production angular distributions to the OPEA curves for a consistent comparison of both charge states of the ρ with the model. This normalization required the ρ^0 production distribution to be

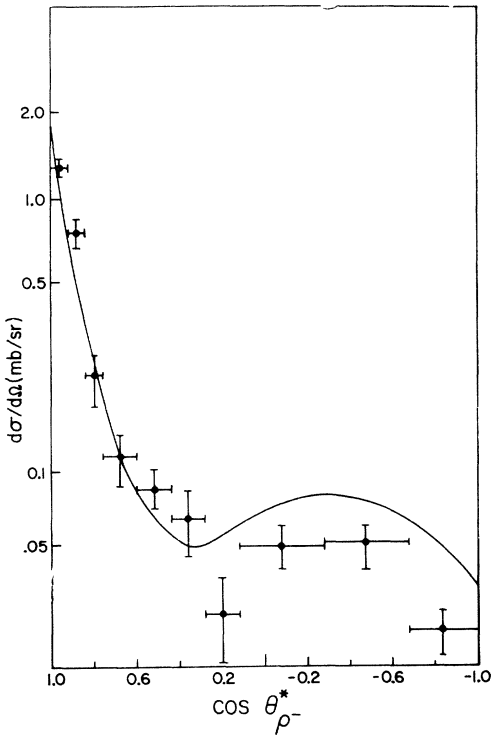

FIG. 19. Semilogarithmic plot of the ρ^- differential production cross section versus $\cos\theta_{\rho^-}{}^*$.

scaled up by a factor of 1.23 and that of the ρ^- to be scaled down by a factor of 0.813. In addition, the nonresonant and isobar backgrounds in the ρ mass region were not subtracted from the data. The chief reason for not subtracting the background is simply a lack of certainty as to its distribution. For experiments at energies of 4 GeV or greater, it is clear that some form of forward-peaking background should be used. At energies lower than ours, a background dominated by s-channel resonances could be used. In this intermediate region, the situation is not so clear-cut. For purposes of simplicity, we chose isotropic behavior for the background and analyzed the effects of the reflection of π-nucleon isobar systems into the mass region 680–880 MeV. With this simplified assumption, we obtained a background for Figs. 17 and 18 which was essentially isotropic at about two events per interval. The true background might be nonuniform in its distribution and larger in magnitude. This possibility must be kept in mind when interpreting Figs. 17–20, where background has not been subtracted.

In comparing Fig. 17 with Fig. 18, there may be some question concerning experimental bias against ρ^- events for values of $\cos\theta_\rho{}^*$ close to 1.0; this bias would essentially result from inability of scanners to find short proton tracks. The corresponding bias should not exist for the ρ^0 events because the neutron is never observed. This bias turns out to be serious only for the two intervals farthest to the left in Fig. 17, since at our energy a value of $\cos\theta_\rho{}^*=0.98$ implies a laboratory kinetic energy for the recoil proton equal to about 32 MeV, corresponding to a range of about 5 cm in liquid hydrogen. The data in these intervals are not adjusted for this bias. However, it must be remembered that the smooth curve in Fig. 17 is based on an OPEA calculation using data from our elastic scattering experiments.[28] Hence, the shape of the curve is in no way influenced by the bias in the first two intervals.

In Figs. 19 and 20, we present a semilogarithmic plot of the ρ differential production cross sections for all values of $\cos\theta_\rho{}^*$. Here we have been more selective in our dipion mass selection criterion in an attempt to reduce further the effect of background in the large-angle region of the ρ differential production cross sections. The plots correspond to 353 events with $740\leq M(\pi^-\pi^0)\leq 820$ MeV and 540 events with $720\leq M(\pi^-\pi^+)\leq 800$ MeV. The resulting background in this region is estimated to be 16% for both charge states of the ρ. Three points are of interest with respect to this form of data presentation.

(a) The solid curves in Figs. 19 and 20, in the region $\cos\theta_\rho{}^*\geq 0.75$, are essentially the OPEA-model prediction,[33] and these graphs have the same type of normalization as do Figs. 17 and 18. This presentation of the data is in better apparent agreement with the OPEA

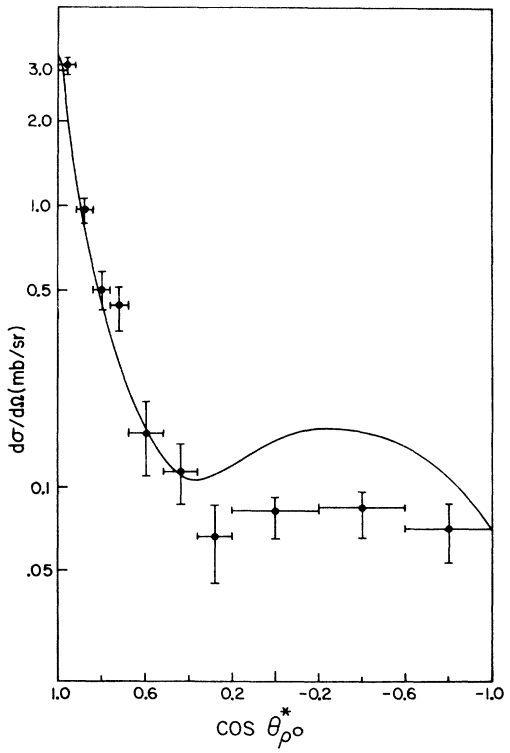

FIG. 20. Semilogarithmic plot of the ρ^0 differential production cross sections versus $\cos\theta_{\rho^0}{}^*$.

[33] J. D. Kimel (unpublished).

model for two reasons. First, the more stringent mass selection yields production angular distributions that are in slightly better agreement with the OPEA-model prediction than were the data of Figs. 17 and 18. Secondly, we note that the larger $\cos\theta_\rho^*$ intervals together with the logarithmic vertical axis in Figs. 19 and 20 tend to obscure some of the fine detail presented in Figs. 17 and 18. We conclude that the OPEA model gives a reasonably good description of our ρ-production angular distributions in the forward direction.

(b) The nearly exponential dependence of the ρ differential production cross sections on $-t$ was fitted to the form $d\sigma/dt \propto e\beta_\rho t$, with the results

$$\beta_{\rho^-}=10.1\pm0.5 \text{ GeV}^{-2},$$
$$\beta_{\rho^0}=10.3\pm0.5 \text{ GeV}^{-2}.$$

The values of β_ρ are the same, within statistical uncertainties, for both charge states of the ρ. These values of β_ρ are also in agreement with similar values determined in this energy region in other experiments.[15]

(c) Allen *et al.* have reported a diffractionlike structure in the ρ-production differential cross sections at 1.7 GeV/c.[21] While the distributions in Figs. 19 and 20 suggest such structure, the effect is not so dramatic in our data. Nevertheless, we examined this structure in terms of a model for ρ production proposed by Kimel,[33] which attempts to explain some of the structures for

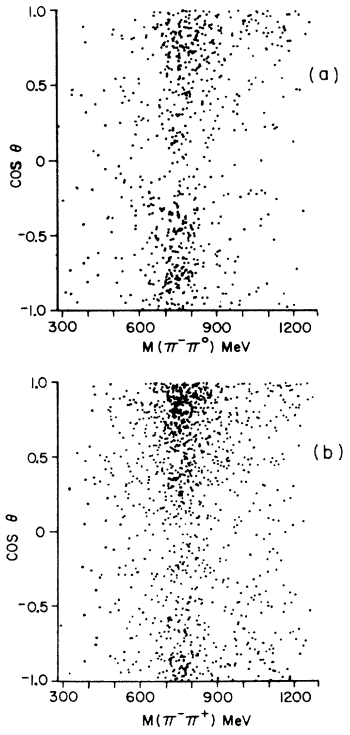

FIG. 21. $\pi\pi$ invariant mass versus $\cos\theta$ with $-t\leq 20\mu^2$: (a) $\pi^-\pi^0 p$, (b) $\pi^-\pi^+ n$.

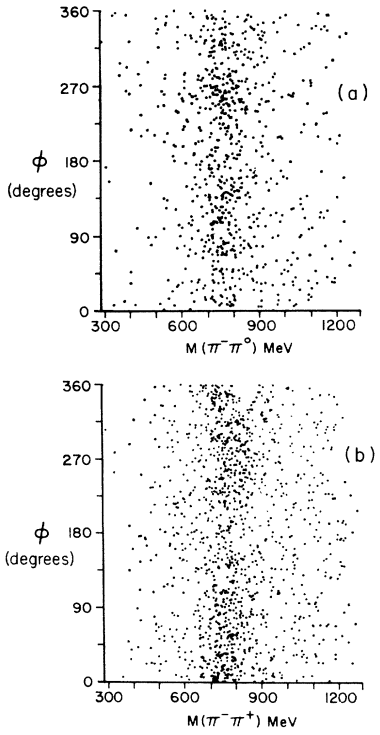

FIG. 22. $\pi\pi$ invariant mass versus ϕ with $-t\leq 20\mu^2$: (a) $\pi^-\pi^0 p$, (b) $\pi^-\pi^+ n$.

$\cos\theta_\rho^*\leq 0.7$ by taking into account the modification in inelastic differential cross sections due to structure in the corresponding elastic differential cross section. This model differs from the conventional formulation of the absorption model for OPE by including nucleon helicity-dependent initial-state and final-state absorption. The initial-state absorption, determined by the elastic S-matrix elements $\eta_{l\pm}$, where $j=l\pm\frac{1}{2}$, was fixed by a fit to our elastic differential cross section[27,28] using the model's parametrization,

$$\eta_{l\pm}=1-\alpha e^{-l^2/L_1^2}-(1-\alpha)e^{-l^2/L_2^2}-\gamma_\pm e^{-(l-L_1)^2/\Delta_1^2}. \quad (8)$$

The initial-state absorption parameters yielding the best fit to the elastic data ($\chi^2=37$ and 37 data points) are $R_1=0.91$ F, $R_2=0.44$ F, $\alpha=0.25$, $d_1=0.25$ F, $\gamma_+=0.0$, $\gamma_-=0.52$, where $kR_1\equiv L_1+\frac{1}{2}$, $kR_2\equiv L_2+\frac{1}{2}$, $kd_1\equiv\Delta_1$, and k is the c.m. momentum of the initial state. The model assumes that the final-state elastic S-matrix elements also can be approximated by Eq. (8). The final-state absorption parameters are taken to be equal to those of the initial state except that $(R_1)_f=1.1$ F, corresponding to a steeper ρ-nucleon diffraction peak, and $(\alpha)_f=1.0$, corresponding to somewhat stronger absorption of the low partial waves in the final-state elastic scattering. It should be noted that the fourth term of Eq. (8) and the magnitude of γ_- imply that there are sizable helicity-flipping effects which take place on the *surface* of the interaction region. Corre-

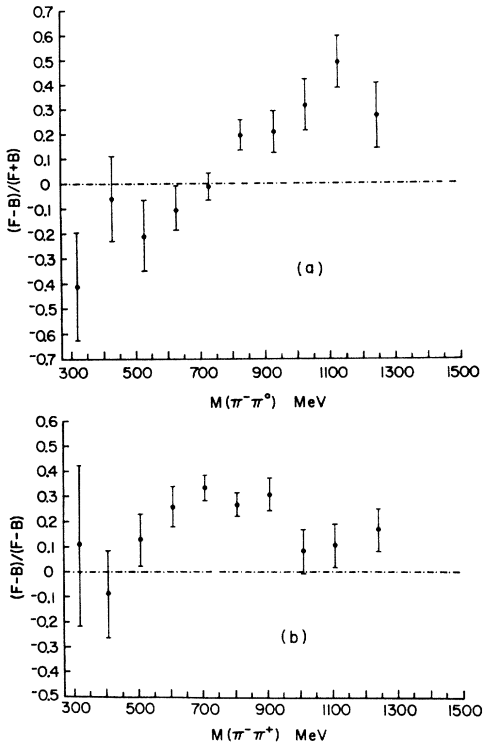

FIG. 23. Forward-backward asymmetry parameter with $-t\leq 20\mu^2$: (a) $\pi^-\pi^0 p$, (b) $\pi^-\pi^+ n$.

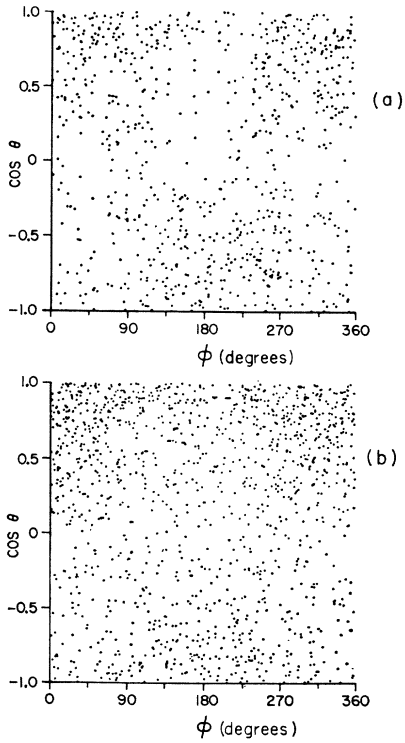

FIG. 24. $\cos\theta$ versus ϕ: (a) $\pi^-\pi^0 p$, (b) $\pi^-\pi^+ n$.

spondingly, there is a sizable effect on the inelastic scattering via the absorption model. The predictions of this model are the solid curves shown in Figs. 19 and 20.

B. ρ-Meson Decay

The ρ-decay angular distributions are most conveniently studied in terms of the two canonical angles θ and ϕ.[34] These angles are defined in the rest frame of the two final-state pions by the following coordinate system: The z axis is the direction of the incident pion and the y axis is the normal to the production plane.

The general features of these decay angular distributions as a function of dipion mass are displayed in Figs. 21 and 22. Here we have plotted only those events with $-t\leq 20\mu^2$. Figure 21 clearly shows a variation of $\cos\theta$ with $M(\pi\pi)$ for both final states. The forward-backward asymmetry $(F-B)/(F+B)$ as a function of dipion mass is given in Fig. 23 for $-t\leq 20\mu^2$. Here F is the number of events with $\cos\theta>0$ and B the number with $\cos\theta<0$. The correlation of $\cos\theta$ and ϕ is plotted in Fig. 24.

In order to compare the ρ-decay angular distributions with the OPEA model, we discuss the two charge states of the ρ separately.

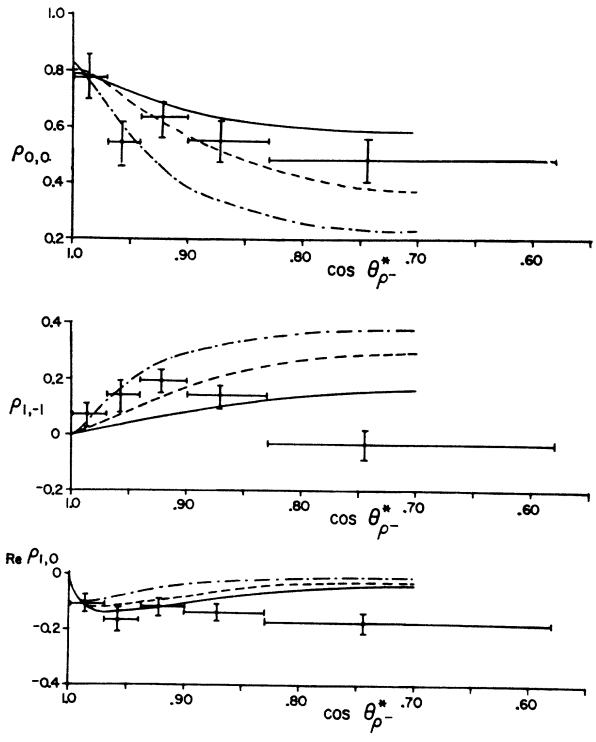

FIG. 25. ρ^- spin-density matrix elements as a function of $\cos\theta_{\rho^-}$*. The solid curve is the OPEA-model prediction. The dashed and dot-dashed curves correspond to $\xi=0.5$ and $\xi=1.0$, respectively.

[34] K. Gottfried and J. D. Jackson, Nuovo Cimento 33, 309 (1964).

TABLE V. Values of the ρ^- spin-density matrix elements as a function of $\cos\theta_{\rho^-}{}^*$.

$\cos\theta_{\rho^-}{}^*$	1.000–0.971	0.971–0.943	0.943–0.900	0.900–0.829	0.829–0.582
$\rho_{0,0}$	$0.78_{-0.08}{}^{+0.08}$	$0.55_{-0.08}{}^{+0.07}$	$0.64_{-0.08}{}^{+0.05}$	$0.55_{-0.08}{}^{+0.07}$	$0.48_{-0.08}{}^{+0.08}$
$\rho_{1,-1}$	$0.07_{-0.04}{}^{+0.04}$	$0.14_{-0.06}{}^{+0.06}$	$0.20_{-0.05}{}^{+0.03}$	$0.14_{-0.05}{}^{+0.04}$	$-0.04_{-0.03}{}^{+0.05}$
$\mathrm{Re}\rho_{1,0}$	$0.11_{-0.03}{}^{+0.03}$	$-0.17_{-0.04}{}^{+0.04}$	$-0.12_{-0.02}{}^{+0.03}$	$0.14_{-0.02}{}^{+0.03}$	$-0.18_{-0.03}{}^{+0.04}$

1. ρ^- Decay

The expected decay distribution for a vector meson decaying into two pions can be parametrized in terms of the spin-density matrix elements as [34]

$$W(\cos\theta,\phi)=(3/4\pi)(\rho_{0,0}\cos^2\theta+\rho_{1,1}\sin^2\theta -\rho_{1,-1}\sin^2\theta\cos2\phi-\sqrt{2}\,\mathrm{Re}\rho_{1,0}\sin2\theta\cos\phi). \quad (9)$$

The elements $\rho_{0,0}$ and $\rho_{1,1}$ are related by the trace condition that $\rho_{0,0}+2\rho_{1,1}=1$. Thus there are three independent parameters to be determined. The individual angular distributions are obtained by integrating Eq. (9), to obtain

$$W(\cos\theta)=\tfrac{3}{4}[(1-\rho_{0,0})+(3\rho_{0,0}-1)\cos^2\theta], \quad (10)$$

$$W(\phi)=(1/2\pi)[(1+\rho_{1,-1})-4\rho_{1,-1}\cos^2\phi]. \quad (11)$$

It should be noted that Eq. (9) is quite general and does not involve a model for a particular exchange mechanism.

The values of the $\rho_{m,m'}$ were determined for events in the 680–880-MeV dipion mass region as a function of

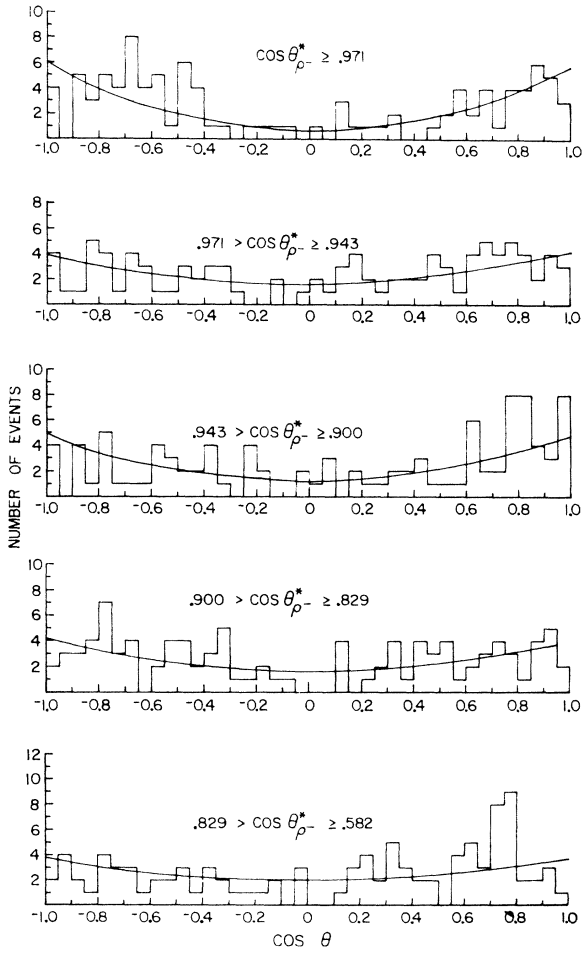

FIG. 26. $\cos\theta$ as a function of $\cos\theta_{\rho^-}{}^*$ for $\pi^-\pi^0 p$ events with $680\leq M(\pi^-\pi^0)\leq 880$ MeV.

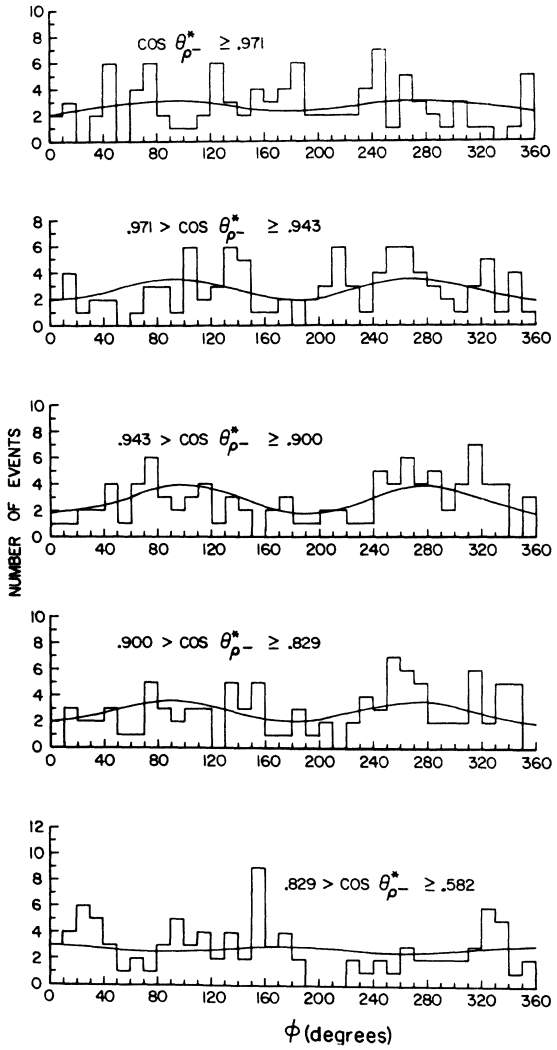

FIG. 27. Treiman-Yang angle ϕ as a function of $\cos\theta_{\rho^-}{}^*$ for $\pi^-\pi^0 p$ events with $680\leq M(\pi^-\pi^0)\leq 880$ MeV.

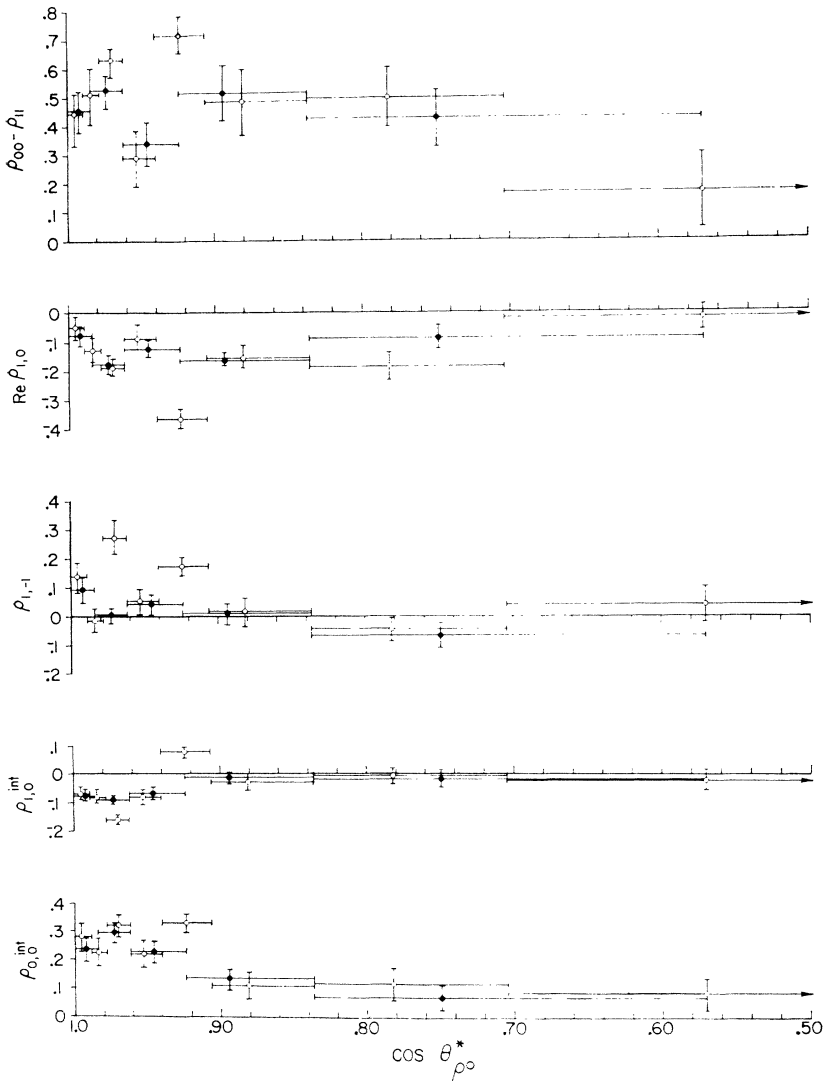

FIG. 28. ρ^0 spin-density matrix elements as a function of $\cos\theta_{\rho^0}$*.

$\cos\theta_\rho$-*. Each $\cos\theta_\rho$-* interval was chosen so that it contained 100 events. The method of maximum likelihood was then used to obtain the values of the $\rho_{m,m'}$. The results of this determination are given in Fig. 25 and Table V. The solid curve in Fig. 25 is the OPEA-model prediction. One can also allow for ω exchange[3] by specifying the appropriate ratio of coupling constants. In this particular case

$$\xi = g_{\pi\rho\omega}(G_{\omega\tilde{\rho}\rho}+G_{\omega\tilde{\rho}\rho})/(2g_{\pi\pi\rho}G_{\pi\tilde{\rho}\rho}). \quad (12)$$

The dashed and dot-dashed curves in Fig. 25 correspond to $\xi=0.5$ and $\xi=1.0$, respectively.[35] A discussion of ω exchange in ρ^- production and of possible $\Delta^0(1236)$ distortion effects in our data has been previously reported.[29] The $\cos\theta$ and ϕ distributions, for events in each $\cos\theta_\rho$-* interval used in the likelihood fitting, are displayed in histogram form in Figs. 26 and 27. The solid curves in each figure are Eqs. (10) and (11) evaluated for the best-fit $\rho_{m,m'}$.

2. ρ^0 Decay

The principal difference between the ρ^- and ρ^0 decay angular distributions is the well-known decay asymmetry of the ρ^0. Durand and Chiu[36] have proposed the existence of a $T=0$, S-wave resonance ϵ^0 with a mass in the ρ^0 region as a possible explanation of the observed asymmetry. Other proposed explanations have consisted of interference with a nonresonant S-wave

[35] These curves were generated for us by R. L. Eisner using a modified version of a program coded by R. Keyser, CERN Report No. DD/co/66/3 (unpublished).

[36] L. Durand, III, and Y. T. Chiu, Phys. Rev. Letters **14**, 329 (1965).

TABLE VI. Values of the ρ^0 spin-density matrix elements as a function of $\cos\theta_{\rho^0}^*$. An interference between the ρ^0 and a $T=0$, S-wave amplitude has been assumed.

$\cos\theta_{\rho^0}^*$	1.000–0.984	0.984–0.962	0.962–0.924	0.924–0.837	0.837–0.570
$\rho_{0,0}-\rho_{1,1}$	$0.46_{-0.08}^{+0.07}$	$0.53_{-0.06}^{+0.05}$	$0.34_{-0.08}^{+0.08}$	$0.52_{-0.10}^{+0.09}$	$0.43_{-0.10}^{+0.09}$
$\mathrm{Re}\rho_{1,0}$	$-0.07_{-0.03}^{+0.03}$	$-0.18_{-0.03}^{+0.03}$	$-0.12_{-0.03}^{+0.03}$	$-0.16_{-0.02}^{+0.03}$	$-0.09_{-0.04}^{+0.04}$
$\rho_{1,1}$	$0.09_{-0.05}^{+0.04}$	$0.00_{-0.02}^{+0.02}$	$0.04_{-0.04}^{+0.03}$	$0.01_{-0.04}^{+0.04}$	$-0.07_{-0.04}^{+0.05}$
$\rho_{1,0}^{\mathrm{int}}$	$-0.07_{-0.02}^{+0.02}$	$-0.09_{-0.01}^{+0.02}$	$-0.07_{-0.02}^{+0.02}$	$-0.01_{-0.02}^{+0.02}$	$-0.02_{-0.03}^{+0.03}$
$\rho_{0,0}^{\mathrm{int}}$	$0.23_{-0.04}^{+0.04}$	$0.30_{-0.04}^{+0.04}$	$0.23_{-0.04}^{+0.04}$	$0.13_{-0.04}^{+0.03}$	$0.07_{-0.05}^{+0.04}$

amplitude.[37–39] Several attempts have been made to observe the ϵ^0 directly, and currently the evidence is running against the existence of such a resonance.[40]

If we assume the existence of a $T=0$, $J=0$ amplitude in addition to the $T=1$, $J=1$ ρ^0 amplitude, the angular distribution may be written

$$W(\cos\theta,\phi)=1/4\pi+(3/4\pi)[(\rho_{0,0}-\rho_{1,1})(\cos^2\theta-\tfrac{1}{3}) -\sqrt{2}\,\mathrm{Re}\rho_{1,0}\sin 2\theta\cos\phi-\rho_{1,-1}\sin^2\theta\cos 2\phi] +(\sqrt{3}/4\pi)(-2\sqrt{2}\,\mathrm{Re}\rho_{1,0}^{\mathrm{int}}\sin\theta\cos\phi +2\,\mathrm{Re}\rho_{0,0}^{\mathrm{int}}\cos\theta). \quad (13)$$

Here ρ^{int} denotes the matrix elements for S-P interference.[41] The individual decay angular distributions, obtained by integration of $W(\cos\theta,\phi)$, are given by

$$W(\cos\theta)=\tfrac{1}{2}[1+(\rho_{0,0}-\rho_{1,1})(3\cos^2\theta-1) +2\sqrt{3}\,\mathrm{Re}\rho_{0,0}^{\mathrm{int}}\cos\theta], \quad (14)$$

$$W(\phi)=(1/2\pi)[1+\rho_{1,1}(1-2\cos^2\phi) -(\tfrac{1}{2}\pi\sqrt{6})\,\mathrm{Re}\rho_{1,0}^{\mathrm{int}}\cos\phi]. \quad (15)$$

In this formulation five parameters must be determined.

The likelihood method was again employed to determine the density-matrix elements with each $\cos\theta_{\rho^0}^*$ interval containing 150 events. The matrix elements were also determined using 100 events per $\cos\theta_{\rho^0}^*$ interval. These results are presented in Fig. 28 and in Table VI. In Fig. 28 the open circles represent the 100-event determination and the solid circles correspond to 150 events per $\cos\theta_{\rho^0}^*$ interval. The purpose of the dual determination was to explore the dip in the $\rho_{0,0}-\rho_{1,1}$ distribution near $\cos\theta_{\rho^0}^*=0.95$. A similar dip is seen to occur in the $\rho_{0,0}$ distribution of the ρ^-.

In view of the fact that we observe evidence for three isobar resonances in the $\pi^+ n$ mass distribution, we examined what effect the presence of these resonances would have on the ρ^0 asymmetry. We find that the presence of these resonances, either individually or collectively, cannot account for the observed asymmetry.

The best-fit forms of Eqs. (14) and (15) are displayed on the individual $\cos\theta$ and ϕ histograms for the 150

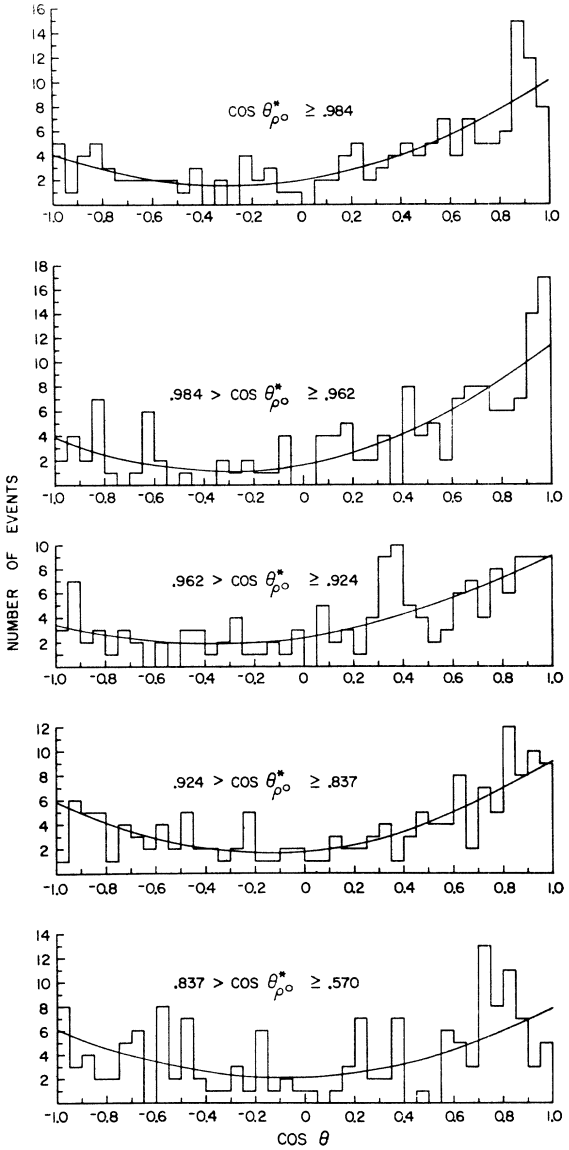

FIG. 29. $\cos\theta$ as a function of $\cos\theta_{\rho^0}^*$ for $\pi^-\pi^+ n$ events with $680\leq M(\pi^-\pi^+)\leq 880$ MeV.

[37] M. M. Islam and R. Piñon, Phys. Rev. Letters **12**, 310 (1964).
[38] S. H. Patil, Phys. Rev. Letters **13**, 261 (1964).
[39] P. G. Turnauer, Phys. Rev. Letters **14**, 985 (1965).
[40] V. Hagopian, W. Selove, J. Alitti, J. P. Baton, and M. Neveu-René, Phys. Rev. Letters **14**, 1077 (1965); M. Feldman, W. Frati, J. Halpern, A. Kanofsky, M. Nussbaum, S. Richert, P. Yamin, S. Choudry, S. Devons, and J. Grunhaus, *ibid.* **14**, 869 (1965); I. P. Corbett, G. J. S. Damerell, N. Middlemas, D. Newton, A. B. Clegg, W. S. C. Williams, and A. S. Carroll, Phys. Rev. **156**, 1451 (1967); M. A. Jabiol, F. E. James, and N. H. Khanh, Phys. Rev. Letters **17**, 1065 (1966); H. O. Cohn, W. M. Bugg, G. T. Condo, R. D. McCulloch, G. Lütjens, and N. Gelfand, *ibid.* **15**, 906 (1965).
[41] P. Csonka and L. Gutay, University of California Lawrence Radiation Laboratory Report No. UCRL-50101, 1966 (unpublished).

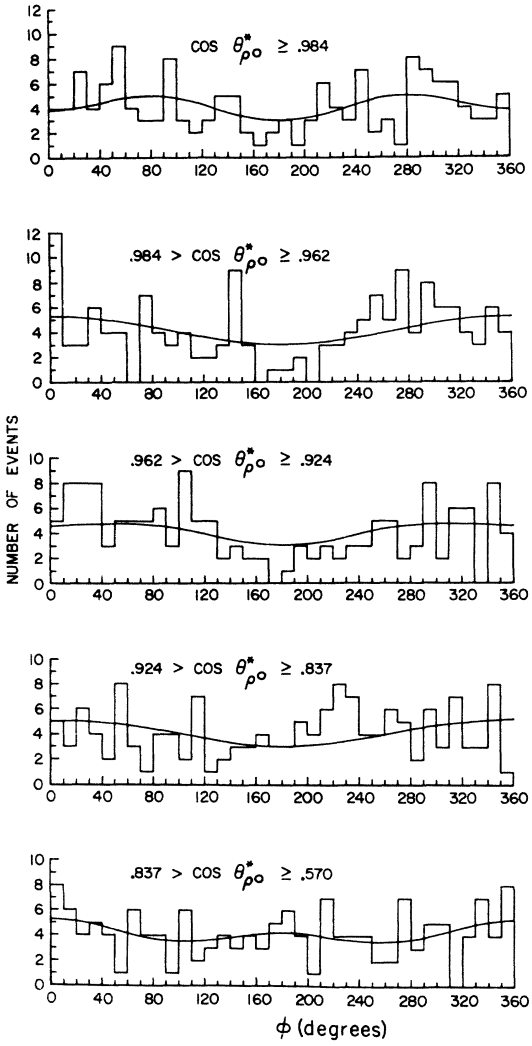

FIG. 30. Treiman-Yang angle ϕ as a function of $\cos\theta_{\rho^0}^*$ for $\pi^-\pi^+$ events with $680 \leq M(\pi^-\pi^+) \leq 880$ MeV.

events per $\cos\theta_{\rho^0}^*$ interval determination in Figs. 29 and 30.

We have also looked for the ϵ^0 following the method suggested by Hagopian *et al.*[40] In Fig. 31 we have plotted $M(\pi^-\pi^+)$ for events with $-t \leq 4\mu^2$. The shaded events correspond to $|\cos\theta| \leq 0.3$. We see no evidence to support the existence of the ϵ^0 in these data, since there is no shift in the mass peak to 720 MeV.

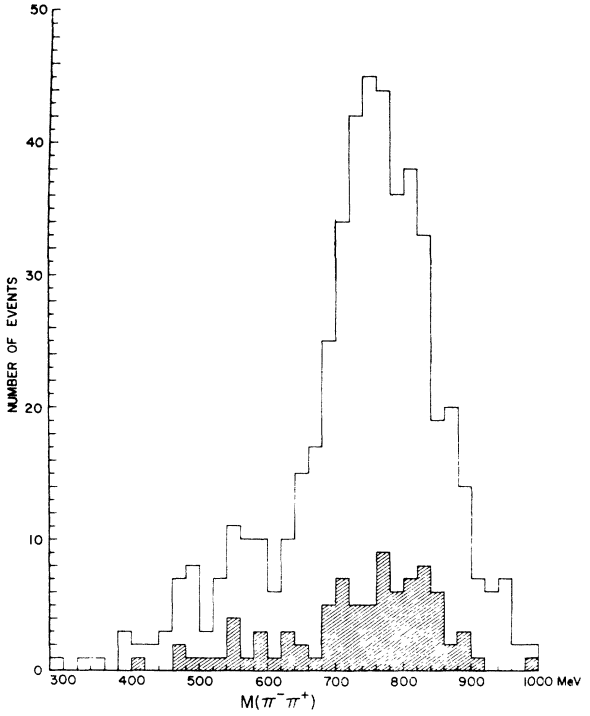

FIG. 31. Effective mass of the $\pi^-\pi^+n$ final state with $-t \leq 4\mu^2$. The shaded events correspond to $-t \leq 4\mu^2$ and $|\cos\theta| \leq 0.3$.

ACKNOWLEDGMENTS

The authors wish to thank the Alvarez group at the Lawrence Radiation Laboratory for providing the film and the PANAL-PACKAGE programs. We especially thank our scanning and measuring staff. In particular, we appreciate the efforts of Mrs. B. J. McLain, Mrs. J. M. Hoover, Mrs. C. A. Alderman, and R. M. Waterson. The assistance of the Florida State University Computing Center is gratefully acknowledged. Many helpful conversations with Professor P. K. Williams have contributed greatly to this paper.